BIOCHEMISTRY
including biophysical chemistry & molecular biology
Article

Biochemistry **2010,** *49,* 2031–2041 2031
DOI: 10.1021/bi9020988

Structural Basis for the Mechanism and Substrate Specificity of Glycocyamine Kinase, a Phosphagen Kinase Family Member[†,‡]

Kap Lim,[§,#] Sadhana Pullalarevu,[§,#] Karen Talin Surabian,[§] Andrew Howard,[∥] Tomohiko Suzuki,[⊥] John Moult,[§] and Osnat Herzberg*[,§]

[§]*Center for Advanced Research in Biotechnology, University of Maryland Biotechnology Institute, Rockville, Maryland 20850,* [∥]*Illinois Institute of Technology, Chicago, Illinois 60616, and* [⊥]*Laboratory of Biochemistry, Faculty of Science, Kochi University, Kochi, Japan* [#]*These authors contributed equally to the studies.*

Received December 7, 2009; Revised Manuscript Received January 28, 2010

ABSTRACT: Glycocyamine kinase (GK), a member of the phosphagen kinase family, catalyzes the Mg^{2+}-dependent reversible phosphoryl group transfer of the *N*-phosphoryl group of phosphoglycocyamine to ADP to yield glycocyamine and ATP. This reaction helps to maintain the energy homeostasis of the cell in some multicelullar organisms that encounter high and variable energy turnover. GK from the marine worm *Namalycastis* sp. is heterodimeric, with two homologous polypeptide chains, α and *β*, derived from a common pre-mRNA by mutually exclusive N-terminal alternative exons. The N-terminal exon of GK*β* encodes a peptide that is different in sequence and is 16 amino acids longer than that encoded by the N-terminal exon of GKα. The crystal structures of recombinant GKα*β* and GK*ββ* from *Namalycastis* sp. were determined at 2.6 and 2.4 Å resolution, respectively. In addition, the structure of the GK*ββ* was determined at 2.3 Å resolution in complex with a transition state analogue, $Mg^{2+}-ADP-NO_3^-$−glycocyamine. Consistent with the sequence homology, the GK subunits adopt the same overall fold as that of other phosphagen kinases of known structure (the homodimeric creatine kinase (CK) and the monomeric arginine kinase (AK)). As with CK, the GK N-termini mediate the dimer interface. In both heterodimeric and homodimeric GK forms, the conformations of the two N-termini are asymmetric, and the asymmetry is different than that reported previously for the homodimeric CKs from several organisms. The entire polypeptide chains of GKα*β* are structurally defined, and the longer N-terminus of the *β* subunit is anchored at the dimer interface. In GK*ββ* the 24 N-terminal residues of one subunit and 11 N-terminal residues of the second subunit are disordered. This observation is consistent with a proposal that the GKα*β* amino acids involved in the interface formation were optimized once a heterodimer emerged as the physiological form of the enzyme. As a consequence, the homodimer interface (either solely α or solely *β* chains) has been corrupted. In the unbound state, GK exhibits an open conformation analogous to that observed with ligand-free CK or AK. Upon binding the transition state analogue, both subunits of GK undergo the same closure motion that clasps the transition state analogue, in contrast to the transition state analogue complexes of CK, where the corresponding transition state analogue occupies only one subunit, which undergoes domain closure. The active site environments of the GK, CK, and AK at the bound states reveal the structural determinants of substrate specificity. Despite the equivalent binding in both active sites of the GK dimer, the conformational asymmetry of the N-termini is retained. Thus, the coupling between the structural asymmetry and negative cooperativity previously proposed for CK is not supported in the case of GK.

Glycocyamine kinase (ATP:guanidinoacetate *N*-phosphotransferase, guanidinoacetate kinase, GK,[1] EC 2.7.3.1) belongs to the family of phosphagen kinases, enzymes that catalyze the Mg^{2+}-dependent reversible conversion of guanidinium-containing substrates and ATP into the respective N^{ω}-phosphorylated substrate and ADP (*1*−*3*). GK acts on glycocyamine (guanidinoacetate) and phosphoglycocyamine (phosphoguanidinoacetate, N^{ω}-phosphonoglycocyamine) (Figure 1). Phosphoglycocyamine and other phosphagens serve as energy reservoirs for rapid regeneration of ATP and for maintaining the energy balance of the cell. Whereas vertebrates produce only one phosphagen kinase, creatine kinase (CK), lower invertebrates produce multiple phosphagen kinases including GK (*4*). Eight phosphagen kinases have been identified in the phyla annelida, CK, arginine kinase (AK), GK, lombricine kinase, thalassemine kinase, taurocyamine kinase, hypotaurocyamine kinase, and opheline kinase (*1*, *4*, *5*). The need for so many phosphagen systems in the same organism is poorly understood. All of these enzymes are thought to have evolved from a common ancestor (*6*). It was proposed that because creatine contains a methyl-substituted

[†]Supported by National Institutes of Health Grant PO1-GM057890. The Advanced Photon Source is supported by the U.S. Department of Energy, Basic Energy Sciences, Office of Science, under Contract W-31-109-Eng-38.
[‡]Protein Data Bank entry codes: 3L2E for the ligand-free GKα*β*; 3L2D for the ligand-free GK*ββ*; 3L2F and 3L2G for the GK*ββ*/transition state analogue complex (split into two entries).
*Corresponding author. Tel: 240-314-6245. Fax: 240-314-6255. E-mail: herzberg@umbi.umd.edu.
[1]Abbreviations: GK, glycocyamine kinase; CK, creatine kinase; AK, arginine kinase; TSA, transition state analogue.

Published on Web 02/01/2010

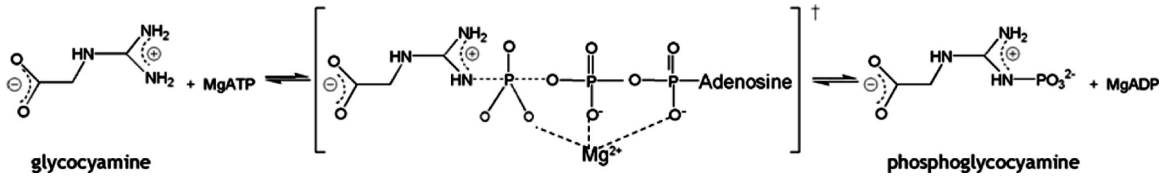

FIGURE 1: Reaction catalyzed by GK.

internal nitrogen atom (guanidino N), the compound is thermodynamically less stable than other phosphagens containing unsubstituted internal N such as glycocyamine or arginine. Thus the latter phosphagens may be preferred over phosphocreatine for ATP production under stress conditions such as acidosis (*7*). The importance of phosphoglycocyamine for immediate energy provision under extreme environmental stress is underscored by the unprecedented high content of this compound in the warm *Nephtys hombergii*, a burrowing predator living in marine sediments (*8*).

Sequence analyses led to the proposal that AK is the oldest phosphagen kinase and CK diverged from it at an early stage of evolution (*9*, *10*). Monomeric AK is the most prevalent phosphagen kinase in invertebrates. Dimeric AK exists in sea cucumber and may have back-evolved from CK (*11*). There are three types of CK, cytosolic (muscle-type and brain-type), mitochondrial, and flagellar (*12*). The cytosolic CK assembles into dimers. Mitochondrial CK is in equilibrium between dimeric and octameric forms (*13*, *14*). Flagellar CK comprises a fused trimer, which is found in many protostome and deuterostome invertebrates and in protochordate.

The GK from marine worms is a dimeric protein that is alternatively spliced at the N-termini of the subunits with the shorter exon encoding the α chain and the 16 amino acid residue longer exon encoding the β chain (*6*). Ellington and colleagues proposed that the ancestral GK was composed of the αα homodimer but alternative splicing occurred possibly to remove the deleterious effect of mutation in the original gene, thus resulting in the GKαβ heterodimeric enzyme currently present in the marine warms. The molecular mass of the α subunit is ~42 kDa, and that of the β subunit is ~44 kDa (*6*). Because of the high level of sequence identity between GK and CK (> 50%), the three-dimensional structures of the two enzymes are expected to be similar.

The crystal structures of various homodimeric vertebrate CKs, with and without bound ligands, show that the N-terminal region is involved in dimer formation (*15*−*20*). With the exception of one example of dimer subunits that are related by perfect crystallographic symmetry and contain N-termini that adopt two alternative conformations (*20*), each of the two CK N-termini adopts a different conformation, which introduces structural asymmetry irrespective of the presence of bound ligand (*15*−*17*, *21*). Structures of rabbit muscle and *Torpedo californica* CKs in complex with the transition state analogue (TSA) Mg^{2+}−ADP−NO_3−creatine revealed an asymmetry: a ligand-free subunit (or bound to only Mg^{2+}−ADP) that adopted an open conformation and a TSA-bound subunit that adopted the closed conformation (*16*, *17*). For the human brain-type CK, both the CK−TSA and CK−ADP complexes exhibited the closed conformation in the ligand-bound subunit and the open conformation in the ligand-free subunit (*21*). The relationship between the N-termini conformational asymmetry to the observed subunit binding asymmetry is unknown, although it was recently proposed that the N-terminal regions play a role in active site communication and catalytic regulation (*17*). The structural asymmetry supports the view that the CK subunits exhibit negative cooperativity (*22*−*25*), whereas other chemical modification experiments and data from deuterium exchange experiments contradict the notion of negative cooperativity in CK (*26*, *27*). The two distinct alternative spliced GK N-termini imply an inherently asymmetric structure, which is confirmed by the crystal structures of both the homodimeric GK$\beta\beta$ and the heterodimeric GKαβ reported here. In contrast to the CK−TSA complexes, GK binds its TSA, Mg^{2+}−ADP−NO_3−glycocyamine, in both active sites, and both subunits exhibit the closed conformation while maintaining the asymmetric dimer interface.

MATERIALS AND METHODS

Cloning, Expression, and Purification. The GK α and β genes were cloned into the pDEST-His-MBP vector, kindly provided by David Waugh (*28*). The genes were amplified from the pMAL-c2/GKα and pMAL-c2/GKβ plasmids (*29*) by PCR using the following primers: GKα, 5′GAGAACCTGTACTTCCAGGGTATGTTTAAGGACTACACTAGGGAGAAATTTGC3′ (forward) and 5′GGGGACCACTTTGTACAAGAAAGCTGGGTTATTATTACTTGGGAATCATGTCATCGATG3′ (reverse); GKβ, 5′GAGAACCTGTACTTCCAGGGTATGGGTTCAGCCATTCAGGATTACT3′ (forward) and 5′GGGGACCACTTTGTACAAGAAAGCTGGGTTATTATTACTTGGGAATCATGTCATCGATG3′ (reverse). Each of these PCR fragments contained an N-terminal tobacco etch virus (TEV) protease cleavage site sequence designed to be inserted between a maltose binding protein (MBP) gene and the respective GK gene. The resulting PCR products were used as templates for a second PCR with the forward primer 5′GGGGACAAGTTTGTACAAAAAAGCAGGCTCGGAGAACCTGTACTTCCAGGGT3′ and the GKα or GKβ reverse primer to anneal an attB1 recognition site. Each of the two resulting PCR fragments were inserted into pDNOR221 (Invitrogen) by recombinational cloning with the BP clonase system using the standard Gateway protocol (Invitrogen). The nucleotide sequence of the entry clones pGKα221 and pGKβ221 were verified by sequencing. The His_6-MBP fusion protein expression vectors were constructed by recombining the GK genes from pGKα221 and pGKβ221 entry vectors to the destination vector pDEST-His-MBP using the LR clonase enzyme (Invitrogen).

Escherichia coli BL21star(DE3) cells transformed with GKα or GKβ were grown in Luria broth (LB) media containing 100 μg/mL ampillicin to $OD_{600\ nm}$ ~ 0.6 at 37 °C, chilled on ice, and induced with 1 mM isopropyl D-thiogalactopyranoside (IPTG) in a shaker maintained at 22 °C. The cells were harvested by centrifugation after 23 h, and the pellet was frozen at −80 °C. The frozen cells were thawed and resuspended in lysis buffer containing 20 mM Tris-HCl (pH 8.5), 100 mM NaCl, 1 mM DTT, and 0.5 mM EDTA in 1× of Bug buster protein extraction reagent (Novagen), benzonase, and protease cocktail for His-tagged proteins (Sigma). The cells were then lysed by sonication

and centrifuged, and the supernatant was applied onto a Ni-NTA column (Qiagen). The bound protein was eluted in a step gradient with 250 mM imidazole-containing buffer. TEV protease was added to the MBP-GK fusion protein solution at 1:200 molar ratio. After 16 h, the reaction mixture was applied onto a second Ni-NTA column to bind the His-tagged cleaved MBP and the His-tagged TEV protease and elute the cleaved GK. The protein was further purified by size exclusion chromatography on Sephacryl S-100 column using 20 mM Tris-HCl (pH 8.5) and 100 mM NaCl. Protein expression level and sample purity were assessed by SDS−PAGE analysis and homogeneity of the purified protein was assessed by native PAGE analysis. The molecular weight was confirmed by MALDI-TOF mass spectrometry. The oligomeric state of the protein was determined by analytical size exclusion chromatography using a Superdex S200 analytical size exclusion column (GE Healthcare) and also by dynamic light scattering using a DynaPro instrument (Protein Solutions).

Crystallization and Data Collection. GK crystals were obtained at room temperature by vapor diffusion in hanging drops. Drops containing equal volumes of protein (at concentration of 10 mg/mL) and reservoir solution were equilibrated against the reservoir solution containing 22% (w/v) polyethylene glycol 3350, 200 mM $NaNO_3$, and 100 mM Tris-HCl (pH 8.0). To obtain GK$\alpha\beta$ crystals, GKα and GKβ solutions were mixed in 1:1 molar ratio just prior to setting up crystallization experiments. Crystals of $0.2 \times 0.2 \times 0.1$ mm^3 size appeared within 1 week. Both GK$\beta\beta$ and GK$\alpha\beta$ yielded crystals useful for X-ray work whereas the GK$\alpha\alpha$ yielded only stacks of thin needles that could not be improved further.

Crystals of GK$\beta\beta$ bound with the TSA comprising glycocyamine, Mg^{2+}, ADP, and NO_3^- were obtained by the vapor diffusion method from reservoir solution containing 22.5% polymethylmetacrylate 2000, 100 mM calcium acetate, and 100 mM Tris-HCl (pH 8). The TSA was added to the protein solution to achieve a final concentration of 5 mM each $MgCl_2$, ADP, and $NaNO_3$, and 1.25 mM glycocyamine. Rod-shaped crystals of $0.1 \times 0.1 \times 0.2$ mm^3 in size appeared within 3 days. Efforts to obtain GK$\alpha\beta$/TSA crystals were unsuccessful.

The crystals were flash-cooled in liquid nitrogen or in liquid propane cooled with liquid nitrogen. The 2.4 Å diffraction data from a ligand-free GK$\beta\beta$ crystal were collected at ~100 K on the home facility consisting of Osmic Max-Flux monochromated X-rays generated by a Rigaku MicroMax 007 rotating anode equipped with a Rigaku AXIS IV^{++} image plate detector. These GK$\beta\beta$ diffraction data were processed with the CrystalClear program (Rigaku/MSC, Woodlands, TX). For the ligand-free GK$\alpha\beta$, 2.6 Å data were collected at the SER-CAT 22BM beamline of the Advanced Photon Source (Argonne National Laboratory, Argonne, IL). The SER-CAT beamline was equipped with a MAR CCD detector. The HKL suite of programs was used to process the GK$\alpha\beta$ diffraction data (*30*). The 2.3 Å resolution diffraction data from a crystal of the GK$\beta\beta$−TSA complex were collected on the SER-CAT 22ID beamline and processed with the XGEN program (*31*). Data collection statistics are provided in Table 1.

Structure Determination and Refinement. The GK$\beta\beta$ structure was determined by the molecular replacement method with the computer program Phaser (*32*, *33*) using a monomer of the chicken brain-type CK crystal structure as the search model (ref *15*; PDB code 1QH4, 56% sequence identity with GK). The N-termini were built de novo because they adopt two different conformations, none of which is similar to that of the CK N-termini. Later, the refined GK$\beta\beta$ structure was used as the search model to obtain a molecular replacement solution for the GK$\alpha\beta$, again with the program Phaser.

Table 1: X-ray Data Collection and Structure Refinement Statistics

	GK$\alpha\beta$	GK$\beta\beta$	GK$\beta\beta$−TSA
data collection			
space group	$P2_1$	$P2_1$	$P2_1$
cell dimensions			
a, *b*, *c* (Å)	84.1, 98.2, 93.1	84.6, 99.7, 93.3	243.1, 114.3, 259.9
β (deg)	91.3	92.4	90.3
no. of dimers in asymmetric unit	4	4	18
solvent content (%)	44	44	46
wavelength (Å)	1.00	1.54	1.00
resolution (Å)	2.6	2.4	2.3
no. of observed reflections	116527	228348	1872589
completeness (%)[a]	90.7 (84.7)	99.6 (99.4)	96.9 (81.2)
no. of unique reflections	42293	60423	610182
R_{merge}[b]	0.085 (0.317)	0.084 (0.344)	0.094 (0.403)
$\langle I/\sigma(I)\rangle$	10.7 (3.4)	11.6 (3.5)	13.8 (3.1)
redundancy	2.8 (2.7)	3.8 (3.7)	3.1 (2.3)
refinement			
no. of reflections used	42274	60171	586126
no. of protein atoms	12034	11833	107131
no. of ligand atoms			1440
no. of water molecules	268	623	6774
R_{cryst}[c]	0.192 (0.293)	0.197 (0.276)	0.197 (0.273)
R_{free}[d]	0.266 (0.371)	0.267 (0.341)	0.263 (0.344)
rmsd from ideal geometry			
bond length (Å)	0.015	0.014	0.009
bond angle (deg)	1.5	1.6	1.3
average *B* factor (Å^2)			
protein	52	43	28
TSA			22
water	49	41	23

[a]The values in parentheses are for the highest resolution shell (2.72−2.60 Å for ligand-free GK$\alpha\beta$, 2.49−2.40 Å for ligand-free GK$\beta\beta$, and 2.38−2.30 Å for GK$\beta\beta$−TSA). [b]$R_{merge} = \sum_{hkl}[(\sum_j|I_j - \langle I\rangle|)/\sum_j|I_j|]$. [c]$R_{cryst} = \sum_{hkl}||F_o| - |F_c||/\sum_{hkl}|F_o|$, where F_o and F_c are the observed and calculated structure factors, respectively. [d]R_{free} is computed from 2118 randomly selected reflections omitted from the refinement for ligand-free GK$\alpha\beta$, 3038 for ligand-free GK$\beta\beta$, and 31024 for GK$\beta\beta$−TSA.

The structure of the GK$\beta\beta$−TSA complex was determined by molecular replacement using Phaser. A search model based on the structure of GK$\beta\beta$ in the unbound form did not yield a useful molecular replacement solution. Instead, the rabbit muscle CK−TSA structure (creatine-containing TSA (*17*)) was modified to generate a search model as follows. The rabbit muscle CK−TSA structure forms an asymmetric dimer with one subunit containing the TSA and exhibiting closed conformation and the second subunit containing only Mg^{2+}−ADP and exhibiting an open conformation. This asymmetric dimer did not yield a useful molecular replacement solution. The search model that produced the molecular replacement solution was obtained by generating a CK dimer in which both subunits adopted the closed conformation and the ligands were omitted to avoid phase bias. The entire asymmetric unit, containing 18 dimers, was built gradually, and the progress of the molecular replacement was assessed by the reduced R_{free} value (< 0.40 when all 18 dimers were placed in the asymmetric unit) and the improved quality of the electron density map.

Structure refinements were performed initially with the CNS program (*34*) followed by either REFMAC (*35*) or PHENIX (*36*). For the ligand-bound GK$\beta\beta$ structure, the R_{free} and R_{work} values were reduced substantially when twinning refinement was applied in PHENIX with the twinning operator ($-h$, $-k$, l). The estimated twinning fraction was 0.31. In contrast, the diffraction data for the substrate-free GK$\alpha\beta$ and GK$\beta\beta$ crystals did not indicate significant twinning, and in both cases the structure refinement was completed with REFMAC. Water molecules were added to account for peaks in the $F_o - F_c$ electron density map higher than 3σ and observed within hydrogen bond distance from protein atoms or other water molecules. Model building and modifications were performed with the interactive graphics programs O (*37*) and COOT (*38*). Refinement statistics are provided in Table 1.

It worth noting that the diffraction data for the crystals of the GK$\beta\beta$−TSA complex were processed in space group $P2_1$, which yields 18 dimers in the asymmetric unit; however, the data could also be processed using the higher symmetry space group, $P2_12_12_1$. Although a molecular replacement solution was obtained also in the orthorhombic cell, the reduced symmetry (coupled with twinning) was required for the structure refinement to progress.

Figures were generated with MOLSCRPT (*39*) followed by RASTER3D (*40*, *41*). Conformational changes were analyzed with the computer program DynDom (*42*).

RESULTS AND DISCUSSION

Note on Sequence Numbering. The GK α and β polypeptide chains are identical except in the N-terminal alternatively spliced segments (*29*):

```
GKα                          MFKDYTREKFAKE.....YE...
GKβ  MGSAIQDYFVKNRVGHSKPWESGKFKAAD.....KE...
          5    10   15   20   25        48
```

Exon 1 of the GK gene encodes the 48 N-terminal amino acids of GKβ, and exon 2 encodes the 32 N-terminal amino acids of GKα. The first residue of the longer β chain is numbered 1, and the first residue of the shorter α chain is numbered 17. As depicted above, the N-terminal sequences of the α and β GK variants differ over the first 29 amino acid residues, the ensuing 17 residues are identical, position 47 differs, and position 48 is identical. Beyond exons 1 and 2, the amino acid sequences of the GK α and β isoforms are encoded by the same exons and are thus identical.

GK Purification. The expression constructs developed for crystallographic studies consist of a TEV protease cleavable His_6-MBP-GK fusion protein, which enables the application of an affinity purification step followed by cleavage of the fusion protein, separation of the His-tagged MBP, the uncleaved fusion protein, and the His-tagged TEV protease from the cleaved GK, and further purification of the GK by size exclusion chromatography. During the size exclusion step, most of the GKαα sample formed high aggregates that were eluted in the void volume while the yield of the dimeric protein was low. In contrast, most of the GK$\beta\beta$ sample was eluted as dimers with high aggregates comprising the minor form. These results are consistent with previous reports that the MBP-GKαα fusion protein was unstable (*29*). The GKαα tendency to aggregate may also account for failure to form diffraction quality crystals. Nevertheless, the analytical size exclusion analysis and the dynamic light scattering of the nonaggregated fractions of both GK variants were consistent with dimeric association. The analytical size exclusion also shows that GK$\alpha\beta$ migrates differently than either of the two homodimers, consistent with spontaneous formation of the heterodimer from a 1:1 mixture of GKαα and GK$\beta\beta$.

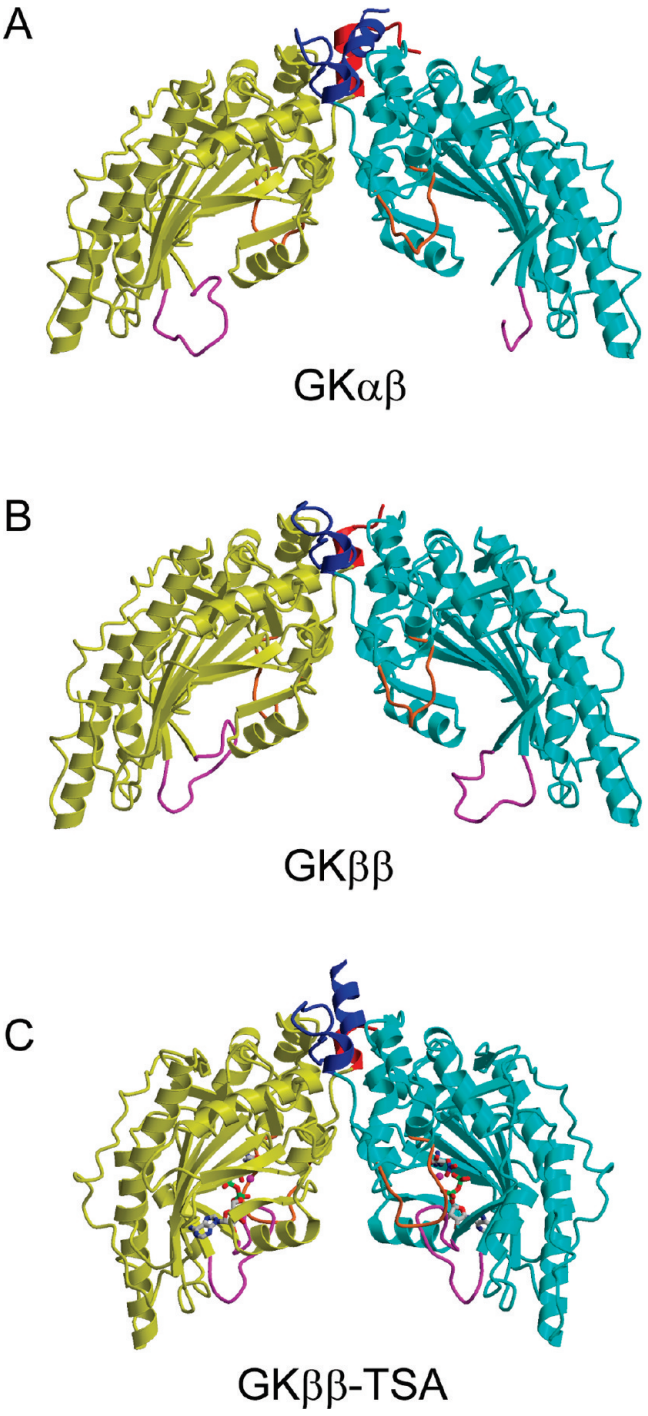

FIGURE 2: Ribbon representations of GK structures. (A) Ligand-free GK$\alpha\beta$ heterodimer. (B) Ligand-free GK$\beta\beta$ homodimer. (C) The GK$\beta\beta$ homodimer bound with glycocyamine, Mg^{2+}, ADP, and NO_3^- (transition state analogue). For each dimer, the α subunit (or the α-equivalent β subunit in the GK$\beta\beta$) is colored yellow, and the β subunit is colored cyan. The N-terminus of the α subunit is colored red, and the N-terminus of the β subunit is colored blue. The phosphagen-specific loop (brown color) and nucleotide-binding loop (magenta color) are far apart in the ligand-free state (A, B) and are placed in close proximity in the ligand-bound structure. The nucleotide-binding loop is partially disordered in the β subunit of the ligand-free GK$\alpha\beta$ (A).

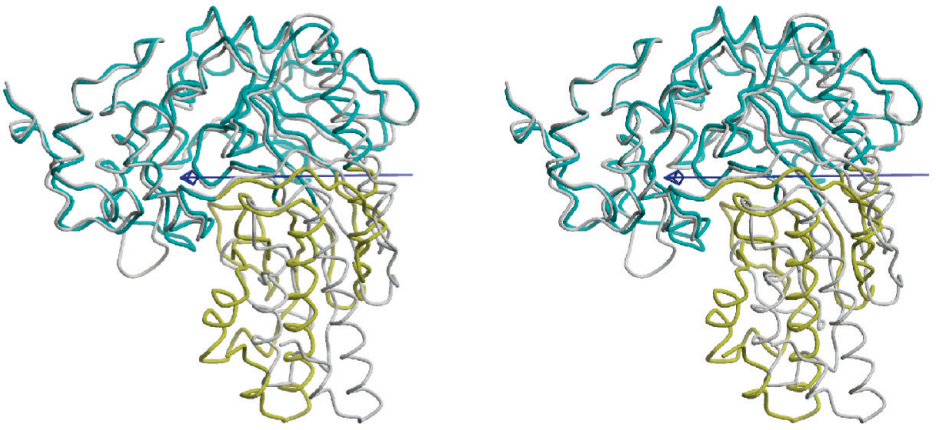

FIGURE 3: Stereoscopic representation of the GK overall conformational change displayed together with the effective hinge calculated by the program DynDom (*42*). The open conformation is depicted in gray color. The fixed domain of the closed conformation is colored cyan, and the moving domain is colored yellow. The arrow corresponds to the effective hinge axis around which the moving domain rotates 22° upon TSA binding.

Overall Structure. The crystals of apo GK$\alpha\beta$ and GK$\beta\beta$ are isomorphous and contain two dimers in the asymmetric unit. Except for the N-termini, which are fully defined in GK$\alpha\beta$ but exhibit some disorder in GK$\beta\beta$ (no interpretable electron density is associated with the 24 N-terminal residues of one subunit and 11 N-terminal residues of the second subunit), the structures are the same (Figure 2A,B). The root-mean-squared deviation (rmsd) of the common α-carbon residues 27−331 and 343−390 is 0.6 Å. As with other phosphagen kinase family members, the molecule consists of an N-terminal α-helical domain (residues 12−114) and a larger C-terminal α/β saddle domain (residues 115−390). The subunits' N-termini form much of the dimer interface, although the C-terminal domain loop residues 156−160 and 220−221 are also involved in subunit contacts. Different in length and sequence, the N-termini of the α and β subunits in the GK$\alpha\beta$ dimer adopt different conformations, which result in an asymmetric interface. Moreover, the two N-termini in the GK$\beta\beta$ homodimer also form an asymmetric interface despite their identical N-termini sequence. As discussed later in more detail, the interfaces of both structures are similar except for the partial disorder in the GK$\beta\beta$ N-termini.

Binding of the TSA Mg^{2+}−ADP−NO_3−glycocyamine to GK$\beta\beta$ (NO_3 mimics a planar phosphoryl group during the phosphotransfer reaction) induces a rigid body like conformational transition that changes the relationship between the α-helical and α/β domains so that the active site crevice is less accessible to bulk solvent and the two lobes of each subunit are closer to one another (Figure 2C). The dimer interface is not affected; thus the rigid body movement is best envisaged as shifting the C-terminal α/β domains with respect to the fixed N-terminal α-helical domains. In the following discussion, we refer to the ligand-free GK conformation as the open conformation and to the enzyme conformation induced by binding of the TSA as the closed conformation.

The computer program DynDom was used to analyze more accurately the quasi rigid body domain motion (*42*). The DynDom analysis yields an effective hinge axis, which is defined as an interdomain screw axis that passes within 3 Å of the Cα atom of any of the interdomain residues involved in the interdomain motion. Using the GK β subunit structure in the open (ligand free) and closed (ligand bound) states, the DynDom analysis defines a fixed domain that encompasses residues 27−115, 141−249, and 264−302, corresponding to the lobe close to the dimer interface. The domain that moves relative to the fixed domain encompasses residues 116−140, 250−263, and 303−388 and corresponds to the lobe remote from the dimer interface. This analysis yielded a 22° rotation around an axis approximately parallel to the dimer interface and traversing the β-sheet underlying the active site crevice (Figure 3). The effective hinge axis has essentially no translation component (0.04 Å). Using DynDom analysis, effective hinge axes also describe the CK and AK conformational transition with 13° and 20° rotation, respectively, and no significant translation component.

Two active site loops, an N-terminal domain loop (residues 75−84) involved in glycocyamine binding (referred to as the phosphagen-specificity loop, Figure 4) and a C-terminal domain loop (residues 333−342) involved primarily in ATP/ADP binding (referred to as the nucleotide-binding loop, Figure 4), are positioned remotely from one another in the open conformation, whereas they interact with one another in the closed conformation (colored brown and magenta, respectively, in Figure 2). In the ligand-free state, the nucleotide-binding loop exhibits multiple conformations, which may arise from the different crystal environments among the four molecules in the asymmetric unit.

TSA Binding. Previous studies demonstrated that the combination of Mg^{2+}, ADP, nitrate, and phosphagen comprises a transition state analogue that inhibits the catalytic activities of phosphagen kinases. In such a TSA, the planar nitrate serves as a mimic of the planar phosphoryl group during phosphotransfer (*43*−*45*). Indeed, this complex was used in crystallographic studies of CKs and AK (*16*, *17*, *21*, *46*−*48*), which confirmed that the nitrate is stationed between the ADP and the phosphagen. We followed the same strategy in studying the structure of the GK−TSA complex, using Mg^{2+}−ADP, nitrate, and glycocyamine (Figure 5). The electron density map showed that both GK$\beta\beta$ subunits contained the bound TSA in all 18 dimers of the crystal asymmetric unit. Superposition of Cα atoms of all dimer combinations resulted in a rmsd value of 0.5 ± 0.2 Å, with 0.9 Å for the largest deviating dimer pair. The structural variability occurs primarily in the C-terminal α-helix that tends to adopt slightly different orientations with respect to the rest of the structure.

In contrast to the GK−TSA complex, where both subunits bind the glycocyamine TSA, the three reported CK−TSA complexes (from rabbit muscle, *T. californica*, and human brain-type) bind the creatine TSA only in one subunit, which

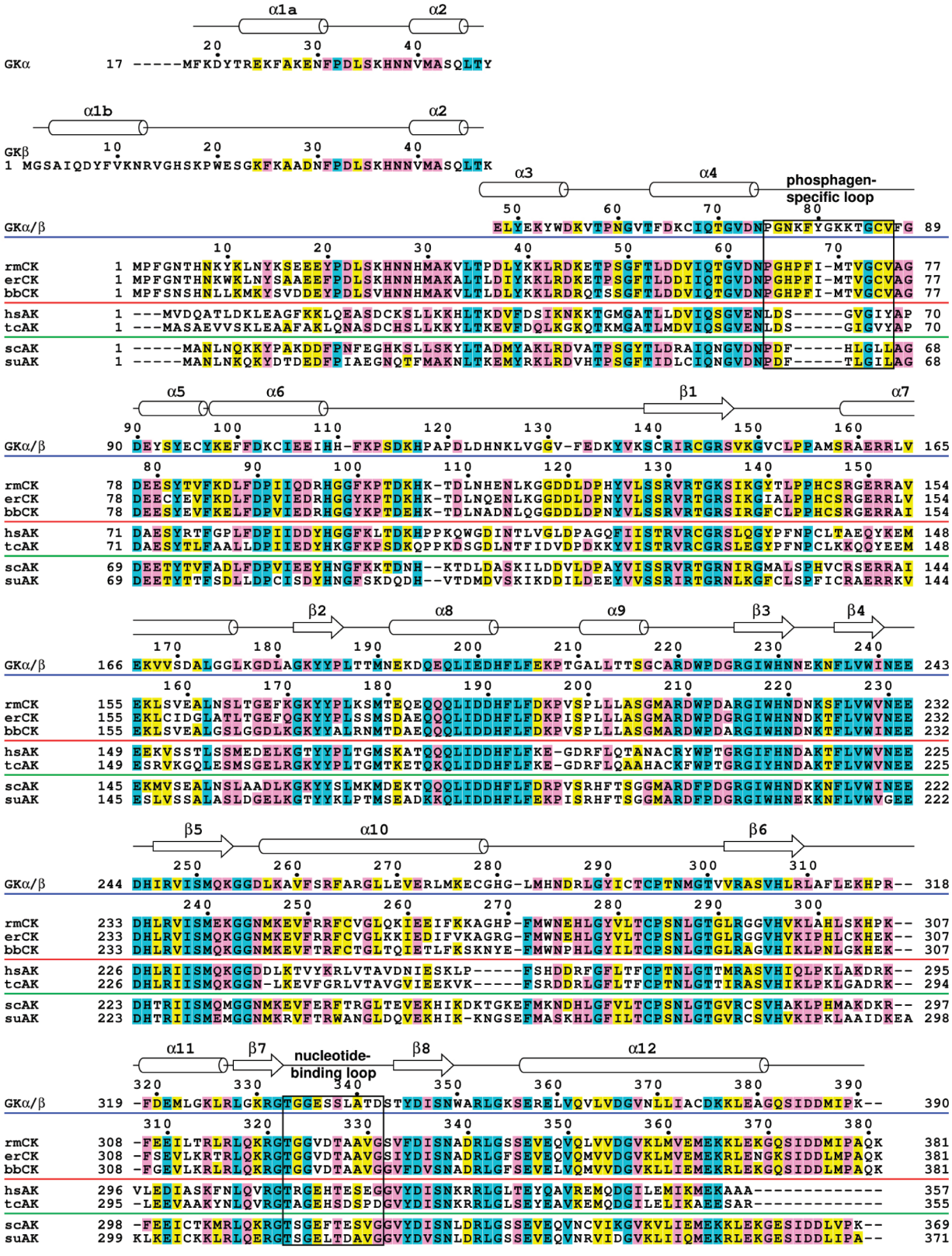

FIGURE 4: Amino acid sequence alignment of GK, CK, and AK. GK secondary structure elements are indicated above the sequence blocks as cylinders for α-helices and arrows for β-strands. The phosphagen-specificity loop and the nucleotide-binding loop are indicated. The GK α and β N-termini sequences are different. Beyond residue 47 (β isoform numbering) the α and β isoforms exhibit identical sequences. The following sequences are aligned below the GK sequence: rabbit muscle CK (rmCK), *T. californica* CK (electric ray, erCK), chicken brain CK (bbCK), horseshoe crab AK (hsAK), *Trypanosoma cruzi* AK (tcAK), sea cucumber (scAK), and sea urchin (suAK). The hsAK and tcAK are monomeric proteins whereas scAK and suAK are dimeric proteins. Residue numbers are provided for AK and CK above the respective block. Amino acid residues are shaded according to BLOSUM62 scores of 3.0 (cyan), 1.5 (pink), and 0.5 (yellow) (*53*).

adopts the closed conformation. The second subunit of the rabbit muscle and *T. californica* binds Mg^{2+}−ADP (*16*, *17*) whereas that of the human brain-type enzyme is ligand-free (*21*). In all of these CK complexes the second subunit adopts the open

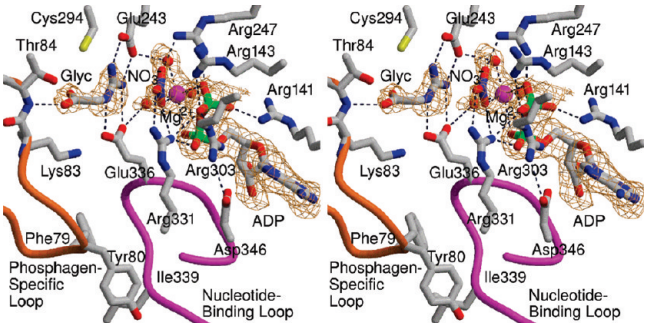

FIGURE 5: Stereoscopic representation of the binding of the TSA (Mg^{2+}−ADP−NO_3−glycocyamine) to GK$\beta\beta$. The $F_o - F_c$ electron density map was calculated prior to the inclusion of the TSA and water molecules in the model and is contoured at 2.5σ level. The phosphagen-specific loop and the nucleotide-binding loop are indicated and colored brown and magenta, respectively. Key interactions with the ADP, NO_3^-, and glycocyamine are shown.

conformation. It is also important to note that, in contrast to the *T. californica* CK−TSA complex, the closed conformation has been recently observed also in the Mg^{2+}−ADP-bound subunit of human brain-type CK (*21*). The asymmetric binding of the TSA to CK has been viewed as supporting the notion of negative cooperativity (*16*), although the mechanism by which this occurs is not clear. The GK structures retain the same asymmetric interface in both the open conformation and when both subunits adopt the closed conformations. Thus there is no structural support for negative cooperativity in this enzyme.

The CK and GK subunits that bind the TSA undergo similar global conformational changes. This is easily discernible when N-terminal domain segments of the TSA-free and TSA-bound molecules are superposed. The N-terminal domain segments encompassing residues 26−76 in GK and residues 14−64 in CK serve as the reference framework in this comparison because they mediate the dimer interface and remain unaltered in the two states. The analysis of the AK conformational change includes a 10 residue shorter N-terminus (residues 24−61) as the reference unit because this monomeric protein contains an N-terminal α-helix absent in GK and CK. The analyses show that the shifts are most pronounced in the phosphagen-specificity loop, α-helices 7 and 8 on the C-terminal domain, and the ensuing β-strand except that the shortest phosphagen-specificity loop of AK does not change upon TSA binding (Figure 6). AK exhibits the greatest displacement of α7 perhaps because it is a monomeric enzyme and not restricted by interaction with a partner subunit (in the dimeric enzymes the N-terminus of α7 is placed in close proximity to the N-terminal region of the partner subunit). Concomitant with the conformational transition of secondary structure units, the side chains of residues that must accommodate these global changes adjust as well, for example, Thr188, Lys207, and Pro208 in GK and the respective Ser178, Lys196, and Pro197 in CK (Figure 6).

In a phosphotransfer that follows the associative mechanism (*49*), the transition state places the transferred phosphorus such that it forms pentagonal bipyramidal geometry with the donor and acceptor groups located in the apical positions ~2 Å from the phosphorus atom. The postulated transition state in the glycocyamine kinase reaction is depicted schematically in Figure 1. The nitrate in the GK−TCA complex mimics the planar phosphoryl group of the transition state (Figures 5 and 6) as its nitrogen atom is positioned approximately midway between the guanidino group of the glycocyamine and the β-phosphoryl of

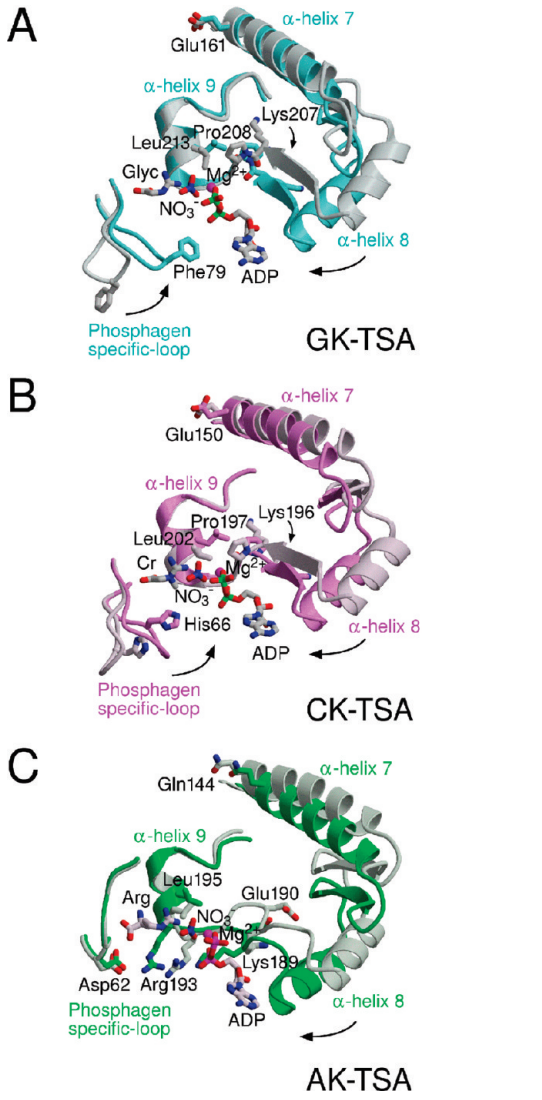

FIGURE 6: Global conformational changes associated with TSA binding in phosphagen kinases. The N-terminal domains in the ligand-free and ligand-bound structures were superposed as described in the text, and shifting structural units in the vicinity of the active site are shown. The arrows depict the direction of movement upon TSA binding.

ADP. Modeling shows that modest rotations around the ADP α- and β-phosphate bonds bring the β-phosphoryl group in line with the nitrate and with a guanidino N atom phosphoryl acceptor of glycocyamine. A similar arrangement occurs in the CK and AK with their respective TSA complexes (Figure 6).

The Mg^{2+} cofactor forms octahedral coordination with the nitrate ion, the P_α and P_β phosphates of ADP, and three water molecules (Figure 5). The coordinating water molecules, in turn, form hydrogen bonds with the carboxylate groups of Glu242, Glu243, and Glu336. Similar Mg^{2+} coordination is present in the CK−TSA and AK−TSA complexes. In addition to the Mg^{2+}, the active site is enriched with arginine residues that interact with the phosphates of ADP and with the NO_3, Arg141, Arg143, Arg247, Arg303, and Arg331 (Figure 5). In turn (not shown in Figure 5), Asp244 interacts with Arg247, Asp346 interacts with Arg303, and Asn297 interacts with Arg143, and all of these residues are conserved in the CK and AK amino acid sequences. Other conserved residues that interact with the nucleotide are His202 that is hydrogen bonded to the ADP ribose C(2)OH and Ser139 that is hydrogen bonded to the adenine's N1. The

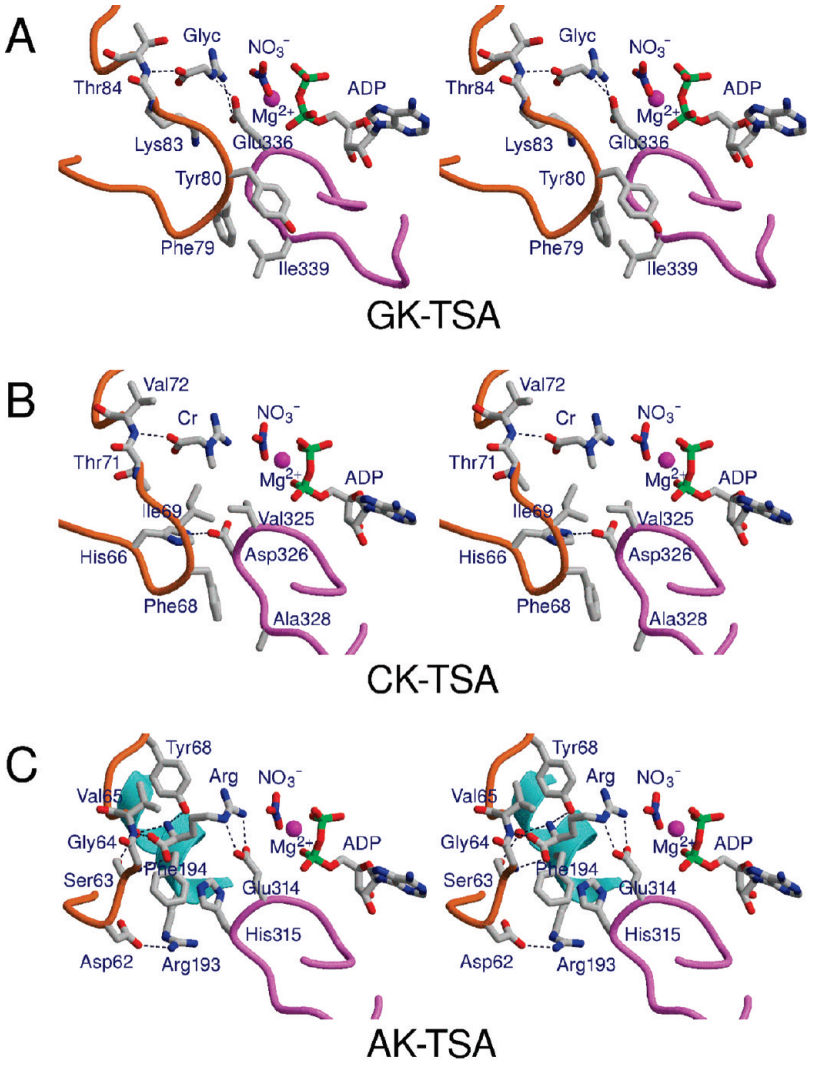

FIGURE 7: Stereoscopic representations showing phosphagen-specific residues in the vicinity of the TSA-bound active sites of (A) GK, (B) CK, and (C) AK. Phosphagen abbreviations used: Glyc, glycocyamine; Cr, creatine; Arg, arginine. The phosphagen-specific loop is colored brown and the nucleotide-binding loop is colored magenta.

interaction of Ser305 with the adenine's NH2 and the N6 occurs also in AK, whereas a glycine residue occupies the same position in CK and instead a water molecule replaces the Ser305 hydroxyl group. The nucleotide-binding loop residues 333−336 flank the ribose and phosphate of ADP and contribute backbone interactions; Thr533 and Gly534 CO groups form hydrogen bonds with the ribose C(2)OH and C(3)OH, respectively. These two residues are conserved to maintain the structural integrity of the nucleotide-binding loop; the Thr533 hydroxyl group is hydrogen bonded to the backbone NH and the hydroxyl group of Thr341, and the backbone of Gly335 (conserved in all phosphagen kinase sequences) adopts dihedral angles that lead to steric strain in C_β-containing residues. Notably, the nucleotide-binding loop is also involved in phosphagen binding specificity through Glu336 as discussed in the following section. Finally, the π-electron stacking interactions of the His307 imidazole ring and Arg141 guanidinium group occur also in CK and AK.

The GK interactions with the glycocyamine are fewer than the interactions with the nucleotide (Figure 5). Two of these interactions are conserved in all phosphagen kinases of known structure; Glu243 and Cys294 interact with the glycocyamine guanidinium group. The glycocyamine carboxylate group forms a hydrogen bond with the backbone NH of Thr84 located on the phosphagen-specific loop, a conserved interaction in CK and AK. The remaining interactions are phosphagen specific. Glu336 interacts with the glycocyamine guanidine group. Lys83 and Thr84 of the phosphagen-specific loop flank the glycocyamine. The Thr84 hydroxyl group is hydrogen bonded with the glycocyamine carboxylate group. The side chain of Lys83 contributes to the sequestering of the glycocyamine from solvent, but its amino group does not form an ion pair with the substrate's carboxyl group.

Determinants of Phosphagen Specificity. Both glycocyamine and arginine lack the internal guanidinium *N*-methyl present in the creatine molecule. A glutamate residue conserved in GK and AK but missing in CK defines the specificity toward a nonsubstituted guanidinium group by engaging it in a salt bridge (Glu336 and Glu314 in GK and AK, respectively). CK displays in the equivalent position a smaller and hydrophobic residue (Val325), which complements the creatine's *N*-methyl substituent (Figure 7) (*16*). The other end of the phosphagen molecule interacts with the phosphagen-specificity loop, which is longest for the smallest phosphagen, glycocyamine, and shortest for the largest phosphagen, arginine (Figures 4 and 7). Here, the interaction of GK and CK with the phosphagen's carboxylate group is the same, employing the Thr84 or Val72 backbone NH,

respectively. A shorter AK loop is required to accommodate the additional four atoms of the arginine substrate. Nevertheless, the backbone interaction with the carboxylate group is conserved in AK (via Val65 NH), and in addition, the Gly64 NH also engages the arginine carboxylate group in a hydrogen bond interaction. In AK, the amino group of the arginine substrate interacts with the Tyr68 hydroxyl group, located on the phosphagen-specific loop, and with an internal water molecule that in turn is hydrogen bonded to Ser63, also an AK phosphagen-specific loop residue. Thus, Tyr68 and Ser63 are determinants of AK activity with the exception of the two dimeric enzymes from the phylum Echinodermata (sea cucumber and sea urchin) where the sequences contain two hydrophobic residues (Phe and Leu) in the analogous positions (Figure 4). Presumably, in these cases the enzymes employ a different strategy to complement the sequestered arginine amino group.

Figure 7 shows that the nucleotide-binding and phosphagen-specific loops in GK and CK interact with one another in the closed conformation. One of the CK conserved phosphagen-specificity loop residues, His66, interacts with the nucleotide-binding loop, Asp326, conserved in all CKs. Site-directed mutagenesis studies of the human CK support the importance of this interaction in catalysis (*50*). In GK, the phosphagen-specificity loop is longer than that of CK or AK. Closure of the GK loops brings Phe79 and Tyr80 on the N-terminal domain in contact with Leu339 on the C-terminal domain, which "locks" the GK closed conformation. These residues are conserved in the few known GK sequences and distinguish the GK from CK.

The short phosphagen-specificity loop of AK does not reach the nucleotide-binding loop (Figure 7C). Instead, both loops exploit interactions with α-helix 9 to establish the closed conformation; Asp62 forms an ion pair with Arg193, and the His315 imidazole ring stacks against the benzene ring of Phe194 (His in the Echinodermata AKs; Figure 4). The GK and CK loops lack equivalent interactions; therefore, the AK Asp62, Arg193, Phe194, and His315 may be considered signature residues of AK activity. Currently, only a few AK sequences have been reported. As more sequences become available, other residue combinations that anchor the loops may emerge, and the validity of these four AK signature residues may need to be revised.

It is important to emphasize that although the structure-based signature residues discussed above help to identify the substrate specificity of phosphagen kinases, by no means is it possible to switch enzyme specificity solely by exchanging the relevant residues. This has been demonstrated by the mutagenesis studies of Jourden et al. (*51*). The authors replaced the CK valine signature residue discussed above by the GK glutamate signature residue and exchanged the phosphagen-specific loop alone or in combination with the Val to Glu replacement. All mutants impaired both CK and GK activities dramatically, and the huge reduction in k_{cat} values rules out conclusions about specificity change. Presumably, as proteins evolve in nature, specificity changes are followed by further sequence changes. Some changes optimize the emerging new activity, and some are random drift from the ancestral molecule, ultimately arriving at a structure that cannot be reversed to perform the ancestral function by simply changing the signature sequences. Indeed, although CK and GK exhibit over 50% sequence identity, there is ample opportunity to drift away from the ancestral enzyme in the remaining residues.

Mutagenesis studies of AK also demonstrate that structures evolve further after function changes occur (*52*). In this case, the entire AK loop containing the Glu314 (analogous to GK Glu336) was replaced with the analogous CK loop, so that position 314 was occupied by a valine, a proposed determinant of CK activity. This replacement and four additional replacements all resulted in smaller side chains compared with the AK amino acid residues. No CK kinase activity was observed whereas the AK activity was reduced only slightly. Apparently, other protein groups that interact with the arginine substrate contribute sufficiently to binding to retain the authentic AK activity. Lacking a crystal structure of the five-residue substituted AK

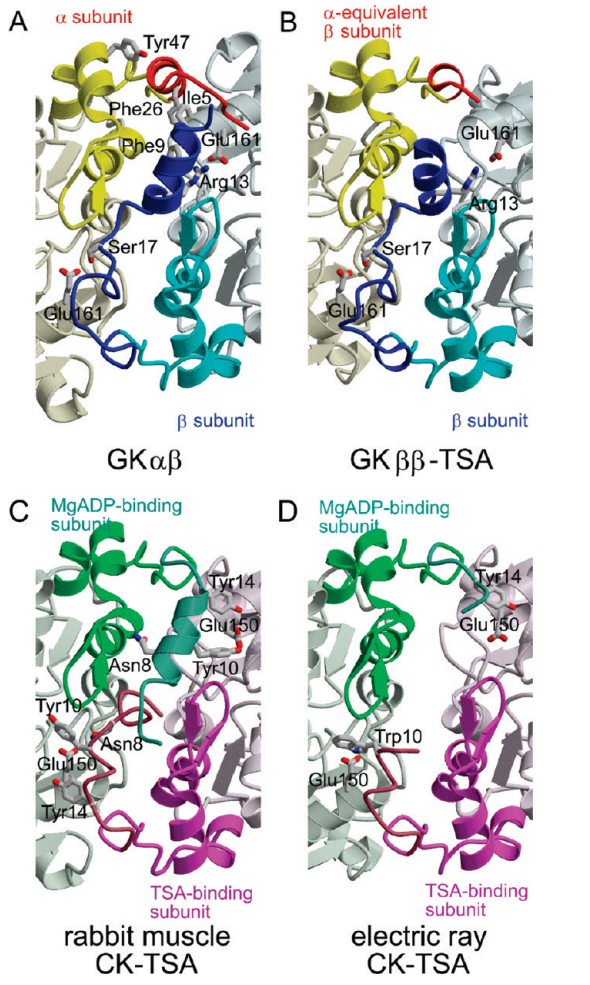

FIGURE 8: N-Termini interactions in the dimer interfaces of phosphagen kinases: (A) ligand-free GKα*β* and (B) GK*ββ*−TSA complex (most ordered dimer). Hydrophobic amino acid residues (Ile5, Phe9, and Phe26) mediate the interaction between neighboring α-helices in GKα*β* (colored blue and red). In GK*ββ*, the two N-termini are incompatible and exhibit more conformational disorder compared with those of GKα*β*. The GK*ββ* α-helix of the chain analogous to the *β* chain in GKα*β* (colored blue) is seen only in 2 out of the 18 dimers in the asymmetric unit of the GK*ββ*−TSA complex, and the *β* chain analogous to the α chain of GKα*β* (colored red) is almost entirely disordered. The interface interaction involving Glu161 is asymmetric in both GK structures (one Glu161 interacts with Arg13 of the same subunit, and the second interacts with Ser17 of the partner subunit). The segments colored in cyan and yellow correspond to N-terminal domain segments of partner subunits that adopt the same conformation and which have been used as reference for structure superposition. (C) Rabbit muscle CK−TSA complex (ref *17*, PDB 1u6r) and (D) *T. californica* CK CK−TSAC (ref *16*, PDB 1vrp). The N-termini of rabbit muscle CK are fully ordered, whereas those of the electric ray CK are partially disordered. Glu150 (a residue equivalent to Glu161 of GK) interacts with the N-termini (of the partner subunit) with the exception of one subunit of the electric ray CK which exhibits more N-terminal disorder.

mutant, it remains unknown whether the grafted loop adopts the same conformation as seen in the CK structure, which would be expected for an enzyme that switches substrate specificity.

The N-Termini Mediate Dimer Assembly. Mutually exclusive alternative splicing of the two N-terminal exons produces the α and *β* variants of GK (Figure 4). The substrate-free GKα*β* heterodimer structure shows that the two N-termini complement one another through hydrophobic interactions that contribute to the dimer interface (Figure 8A). The longer N-terminus of the *β* chain in the GKα*β* structure is fully visible in the electron density map and traverses nearly the entire dimer interface while the shorter N-terminus of the α chain is also fully ordered and located on one side of the dimer interface. The two termini interact only through their respective first α-helices (labeled α1a and α1b in Figure 4) such that Ilu5 and Phe9 of the *β* chain form hydrophobic interactions with Phe26 of the α chain (Figure 8A).

The spontaneous formation of GKα*β* from a 1:1 mixture of GKαα and GK*ββ* suggests that the heterodimer is the most stable form. Indeed, the GKα*β* interface is better packed than the GK*ββ*. The N-termini of the GK*ββ* homodimer exhibit substantial disorder; one chain (the counterpart of the α chain in GKα*β*) is visible only from residue 24 (instead of residue 18 as defined in the α chain of the heterodimeric structure), and the second chain (analogous to the *β* chain of the GKα*β*) is visible only from residue 12. This structural disorder is attributed to the structural incompatibility arising from two identical sequences instead of the complementing α and *β* sequences.

The catalytic rates of GK are comparable with those of CK, and the activity of recombinant GK*ββ* is similar to that of native GKα*β* (*29*). Thus, the disorder of the GK*ββ* N-termini does not affect enzyme activity. In contrast, GKαα tends to aggregate and, in our hands, did not yield single crystals useful for X-ray work. A model of a GKαα dimer using GKα*β* or GK*ββ* as the template for dimer association shows much reduced contact between the two subunits. Thus, if as proposed by Ellington and colleagues the ancestral enzyme consisted of GKαα (*6*), the interface of that ancestral protein could not resemble the current interface.

Interestingly, several but not all dimers in the crystal asymmetric unit of the GK*ββ*−TSA complex (containing 18 dimers) exhibit more order in the interface-traversing *β* chain compared with the corresponding *β* chain of apo GK*ββ*. For two of these dimers, the electron density map accounts the complete α-helix 1b except for the first couple of residues (Figure 8B). This α-helix is misaligned by 25° with the α1b of GKα*β*, presumably because of incompatibility in packing against the N-terminus of the partner *β* chain. As a result of the α-helix shift, Phe9 packs against Trp54 of the partner protein in contrast to GKα*β*, where it is Tyr8 that interacts with Trp54.

The interface-traversing *β* chain in all versions of GK*ββ* and the GK*ββ*−TSA complex is well-defined in the electron density map beginning with Arg13. Arg13 forms a salt bridge with Glu161 of the same *β* subunit, an interaction that is independent of the second subunit (Figure 8A,B). Interactions of residues beyond Arg13 involve the partner subunit beyond residue 47, which are identical in both α and *β* isoforms. The Arg13/Glu161 salt bridge occurs only in one subunit whereas Glu161 of the partner subunit interacts with Ser17; i.e., one Glu161 is involved directly in dimer formation and the second is not (Figure 8A,B).

Both hydrophobic and hydrophilic interactions mediate the contact between the two subunits. There are also water molecules in the interface that bridge the subunits. An intersubunit salt bridge between Asp65 and Arg159 (occurring twice) is a contact conserved in both GK and CK (the corresponding CK residues are Asp54 and Arg148). The Asp/Arg pair is also conserved in the sequences of the dimeric AK from sea cucumber and sea urchin but not in the sequences of the monomeric AK enzymes (Figure 4), which suggests that the presence of these residues may serve to distinguish between dimeric and monomeric phosphagen kinases.

The N-termini of the CK homodimers are also located at the subunit interface, and they are fully or partially ordered in the various structures deposited in the PDB. Two examples of interfaces are depicted in Figure 8C,D. When visible, the arrangement is asymmetric despite the identical sequence of each subunit. Unlike the GKα*β* arrangement, where the N-terminus of the *β* chain mediates most of the intersubunit contacts, the shorter two N-termini of CK mediate intersubunit contacts to the same extent. Nevertheless, the CK residue equivalent to GK Glu161, Glu150, also interacts asymmetrically with the N-terminus except that Glu150 in each subunit interacts with a residue on the partner molecule. For the rabbit muscle CK one Glu150 interacts with Tyr10 (this interaction is not seen in *T. californica* CK because of a larger extent of N-terminal disorder), and the second Glu150 interacts with Asn8 (and with Trp10 in *T. californica* CK) (Figure 8C,D). Taken together, the structural data show that CK and GK evolved different dimerization properties despite the evolutionary relationship they share in terms of sequence, function, overall structure, and the employment of the same dimerization strategy, which exploits the N-termini to generate an asymmetric interface.

ACKNOWLEDGMENT

We thank Buvaneswari Narayanan for help with data collection. We also thank the staff at SER-CAT in Argonne National Laboratory for assistance during the data collection.

REFERENCES

1. Ellington, W. R. (2001) Evolution and physiological roles of phosphagen systems. *Annu. Rev. Physiol. 63*, 289–325.
2. McLeish, M. J., and Kenyon, G. L. (2005) Relating structure to mechanism in creatine kinase. *Crit. Rev. Biochem. Mol. Biol. 40*, 1–20.
3. Suzuki, T., and Furukohri, T. (1994) Evolution of phosphagen kinase: primary structure of glycocyamine kinase and arginine kinase from invertebrates. *J. Mol. Biol. 237*, 353–357.
4. Morrison, J. F. (1973) Arginine kinase and other invertebrate guanidino kinases, in The Enzymes (Boyer, P. C., Ed.) pp 457−486, Academic Press, New York.
5. Van Thoai, N. (1968) Homologous phosphagen phosphokinases, in Homologous Enzymes and Biochemical Evolution (Van Thoai, N., and Roche, J., Eds.) pp 199−229, Gordon and Breach, New York.
6. Ellington, W. R., Yamashita, D., and Suzuki, T. (2004) Alternative splicing produces transcripts coding for alpha and beta chains of a hetero-dimeric phosphagen kinase. *Gene 334*, 167–174.
7. Ellington, W. R. (1989) Phosphocreatine represents a thermodynamic and functional improvement over other muscle phosphagens. *J. Exp. Biol. 143*, 144–194.
8. Arndt, C., and Schiedek, D. (1997) *Nephtys hombergii*, a free-living predator in marine sediments: energy production under environmental stress. *Mar. Biol. 129*, 643–650.
9. Sona, S., Suzuki, T., and Ellington, W. R. (2004) Cloning and expression of mitochondrial and protoflagellar creatine kinases from a marine sponge: implications for the origin of intracellular energy transport systems. *Biochem. Biophys. Res. Commun. 317*, 1207–1214.
10. Tanaka, K., Uda, K., Shimada, M., Takahashi, K., Gamou, S., Ellington, W. R., and Suzuki, T. (2007) Evolution of the cytoplasmic and mitochondrial phosphagen kinases unique to annelid groups. *J. Mol. Evol. 65*, 616–625.
11. Suzuki, T., Kamidochi, M., Inoue, N., Kawamichi, H., Yazawa, Y., Furukohri, T., and Ellington, W. R. (1999) Arginine kinase evolved

twice: evidence that echinoderm arginine kinase originated from creatine kinase. *Biochem. J. 340*, 671–675.
12. Suzuki, T., Mizuta, C., Uda, K., Ishida, K., Mizuta, K., Sona, S., Compaan, D. M., and Ellington, W. R. (2004) Evolution and divergence of the genes for cytoplasmic, mitochondrial, and flagellar creatine kinases. *J. Mol. Evol. 59*, 218–226.
13. Pineda, A. O., and Ellington, W. R. (1999) Structural and functional implications of the amino acid sequences of dimeric, cytoplasmic and octameric mitochondrial creatine kinases from a protostome invertebrate. *Eur. J. Biochem. 264*, 67–73.
14. Kaldis, P., and Wallimann, T. (1995) Functional differences between dimeric and octameric mitochondrial creatine kinase. *Biochem. J. 308*, 623–627.
15. Eder, M., Schlattner, U., Becker, A., Wallimann, T., Kabsch, W., and Fritz-Wolf, K. (1999) Crystal structure of brain-type creatine kinase at 1.41 Å resolution. *Protein Sci. 8*, 2258–2269.
16. Lahiri, S. D., Wang, P. F., Babbitt, P. C., McLeish, M. J., Kenyon, G. L., and Allen, K. N. (2001) The 2.1 Å structure of *Torpedo californica* creatine kinase complexed with the ADP-Mg(2+)-NO(3)-(−)-creatine transition-state analogue complex. *Biochemistry 41*, 13861–13867.
17. Ohren, J. F., Kundracik, M. L., Borders, C. L., Edmiston, P., and Viola, R. E. (2007) Structural asymmetry and intersubunit communication in muscle creatine kinase. *Acta Crystallogr. D63*, 381–389.
18. Rao, J. K., Bujacz, G., and Wlodawer, A. (1998) Crystal structure of rabbit muscle creatine kinase. *FEBS Lett. 439*, 133–137.
19. Shen, Y. Q., Tang, L., Zhou, H. M., and Lin, Z. J. (2001) Structure of human muscle creatine kinase. *Acta Crystallogr. 57*, 1196–1200.
20. Tisi, D., Bax, B., and Loew, A. (2001) The three-dimensional structure of cytosolic bovine retinal creatine kinase. *Acta Crystallogr. 57*, 187–193.
21. Bong, S. M., Moon, J. H., Nam, K. H., Lee, K. S., Chi, Y. M., and Hwang, K. Y. (2008) Structural studies of human brain-type creatine kinase complexed with the ADP-Mg^{2+}-NO_3^--creatine transition-state analogue complex. *FEBS Lett. 582*, 3959–3965.
22. Degani, C., and Degani, Y. (1980) Further evidence for nonsymmetric subunit association and intersubunit cooperativity in creatine kinase. Subunit-selective modifications by 2,4-dinitrophenylthiocyanate. *J. Biol. Chem. 255*, 8221–8228.
23. Degani, Y., and Degani, C. (1979) Subunit-selective chemical modifications of creatine kinase. Evidence for asymmetrical association of the subunits. *Biochemistry 18*, 5917–5923.
24. Hornemann, T., Rutishauser, D., and Wallimann, T. (2000) Why is creatine kinase a dimer? Evidence for cooperativity between the two subunits. *Biochim. Biophys. Acta 1480*, 365–373.
25. Nevinsky, G. A., Ankilova, V. N., Lavrik, O. I., Mkrtchyan, Z. S., Nersesova, L. S., and Akopyan, J. I. (1982) Functional non-identity of creatine kinase subunits of rabbit skeletal muscle. *FEBS Lett. 149*, 36–40.
26. Mazon, H., Marcillat, O., Forest, E., and Vial, C. (2003) Changes in MM-CK conformational mobility upon formation of the ADP-Mg-(2+)-NO(3)(−)-creatine transition state analogue complex as detected by hydrogen/deuterium exchange. *Biochemistry 42*, 13596–13604.
27. Wang, X. C., Zhou, H. M., Wang, Z. X., and Tsou, C. L. (1990) Is the subunit the minimal function unit of creatine kinase? *Biochim. Biophys. Acta 1039*, 313–317.
28. Nallamsetty, S., Austin, B. P., Penrose, K. J., and Waugh, D. S. (2005) Gateway vectors for the production of combinatorially-tagged His6-MBP fusion proteins in the cytoplasm and periplasm of *Escherichia coli*. *Protein Sci. 14*, 2964–2971.
29. Mizuta, C., Tanaka, K., and Suzuki, T. (2005) Isolation, characterization, and cDNA-derived amino acid sequence of glycocyamine kinase from the tropical marine worm Namalycastis sp. *Comp. Biochem. Physiol. B 140*, 387–393.
30. Otwinowski, Z., and Minor, W. (1997) Processing of X-ray diffraction data collected in oscillation mode. *Methods Enzymol. 276*, 307–326.
31. Howard, A. J. (2000) Data processing in macromolecular crystallography, in Crystallographic Computing 7: Proceedings from the Macromolecular Crystallographic Computing School (Bourne, P. E., and Watenpaugh, K. D., Eds.) Oxford University Press, Oxford.
32. McCoy, A. J., Grosse-Kunstleve, R. W., Storoni, L. C., and Read, R. J. (2005) Likelihood-enhanced fast translation functions. *Acta Crystallogr. D61*, 458–464.
33. Storoni, L. C., McCoy, A. J., and Read, R. J. (2004) Likelihood-enhanced fast rotation functions. *Acta Crystallogr. D60*, 432–438.
34. Brunger, A. T., Adams, P. D., Clore, G. M., DeLano, W. L., Gros, P., Grosse-Kunstleve, R. W., Jiang, J. S., Kuszewski, J., Nilges, M., Pannu, N. S., Read, R. J., Rice, L. M., Simonson, T., and Warren, G. L. (1998) Crystallography and NMR system: A new software suite for macromolecular structure determination. *Acta Crystallogr. D54*, 905–921.
35. Winn, M. D., Isupov, M. N., and Murshudov, G. N. (2001) Use of TLS parameters to model anisotropic displacements in macromolecular refinement. *Acta Crystallogr. D57*, 122–133.
36. Adams, P. D., Grosse-Kunstleve, R. W., Hung, L. W., Ioerger, T. R., McCoy, A. J., Moriarty, N. W., Read, R. J., Sacchettini, J. C., Sauter, N. K., and Terwilliger, T. C. (2002) PHENIX: building new software for automated crystallographic structure determination. *Acta Crystallogr. D58*, 1948–1954.
37. Jones, T. A. (2004) Interactive electron-density map interpretation: from INTER to O. *Acta Crystallogr. D60*, 2115–2125.
38. Emsley, P., and Cowtan, K. (2004) Coot: model-building tools for molecular graphics. *Acta Crystallogr. 60*, 2126–2132.
39. Kraulis, P. J. (1991) A program to produce both detailed and schematic plots of protein structures. *J. Appl. Crystallogr. 24*, 946–950.
40. Bacon, D. J. (1988) A fast algorithm for rendering space-filling molecule pictures. *J. Mol. Graphics 6*, 219–220.
41. Merritt, E. A., and Bacon, D. J. (1997) Raster3D: Photorealistic molecular graphics. *Methods Enzymol. 277*, 505–524.
42. Hayward, S., and Berendsen, H. J. (1998) Systematic analysis of domain motions in proteins from conformational change: new results on citrate synthase and T4 lysozyme. *Proteins 30*, 144–154.
43. Held, B. C., Wright-Weber, B., and Grossman, S. H. (2007) Kinetic analysis of two purified forms of arginine kinase: absence of cooperativity in substrate binding of dimeric phosphagen kinase. *Comp. Biochem. Physiol. B 148*, 6–13.
44. Milner-White, E. J., and Watts, D. C. (1971) Inhibition of adenosine 5′-triphosphate-creatine phosphotransferase by substrate-anion complexes. *Biochem. J. 122*, 727–740.
45. Borders, C. L., Snider, M. J., Wolfenden, R., and Edmiston, P. L. (2002) Determination of the affinity of each component of a composite quaternary transition-state analogue complex of creatine kinase. *Biochemistry 41*, 6995–7000.
46. Yousef, M. S., Clark, S. A., Pruett, P. K., Somasundaram, T., Ellington, W. R., and Chapman, M. S. (2003) Induced fit in guanidino kinases—comparison of substrate-free and transition state analog structures of arginine kinase. *Protein Sci. 12*, 103–111.
47. Yousef, M. S., Fabiola, F., Gattis, J. L., Somasundaram, T., and Chapman, M. S. (2002) Refinement of the arginine kinase transition-state analogue complex at 1.2 Å resolution: mechanistic insights. *Acta Crystallogr. 58*, 2009–2017.
48. Zhou, G., Somasundaram, T., Blanc, E., Parthasarathy, G., Ellington, W. R., and Chapman, M. S. (1998) Transition state structure of arginine kinase: implications for catalysis of bimolecular reactions. *Proc. Natl. Acad. Sci. U.S.A. 95*, 8449–8454.
49. Knowles, J. R. (1980) Enzyme-catalyzed phosphoryl transfer reactions. *Annu. Rev. Biochem. 49*, 877–919.
50. Wang, P. F., Flynn, A. J., McLeish, M. J., and Kenyon, G. L. (2005) Loop movement and catalysis in creatine kinase. *IUBMB Life 57*, 355–362.
51. Jourden, M. J., Clarke, C. N., Palmer, A. K., Barth, E. J., Prada, R. C., Hale, R. N., Fraga, D., Snider, M. J., and Edmiston, P. L. (2007) Changing the substrate specificity of creatine kinase from creatine to glycocyamine: evidence for a highly evolved active site. *Biochim. Biophys. Acta 1774*, 1519–1527.
52. Azzi, A., Clark, S. A., Ellington, W. R., and Chapman, M. S. (2004) The role of phosphagen specificity loops in arginine kinase. *Protein Sci. 13*, 575–585.
53. Sonnhammer, E. L., and Hollich, V. (2005) Scoredist: a simple and robust protein sequence distance estimator. *BMC Bioinf. 6*, 108.